



Viscoelastic model to capture residual stresses in heat cured dissimilar adhesive bonded joints

Akshat Agha^{*}, Fadi Abu-Farha

Clemson University - International Center for Automotive Research, Greenville, SC, USA



ARTICLE INFO

Keywords:
 Curing kinetics
 Structural adhesives
 Multi-material joints
 Dissimilar joints
 Residual stress
 Viscoelastic
 DSC
 DMA
 Body-in-White
 BIW

ABSTRACT

The thermal loading during the curing process of an adhesive-bonded joint induces residual stresses in the joint, thereby affecting its performance. The problem becomes worse in the case of a multi-material joint involving varying coefficients of thermal expansion (CTE) for different parts. A novel approach was developed to model the properties of automotive grade structural adhesives during the heat curing process. The material model was divided into two components: curing kinetics model and viscoelastic mechanical model. The models were calibrated using experimental data from Differential Scanning Calorimetry (DSC) and Dynamic Mechanical Analysis (DMA) tests performed on an epoxy-based single-component adhesive. The calibrated material model parameters were fed into a finite element simulation and the prediction results were compared to a unique set of experiments utilizing two substrate combinations of adhesive-bonded single lap shear joints. An excellent agreement between the simulated and experimental results (displacement across the bond, force applied by the adhesive) was achieved. The modeling results give a better understanding of the residual stresses and agree with the experimental trend on the effect of bondline thickness on the joint.

1. Introduction

1.1. Background and literature survey

In recent years, adhesive bonding has emerged as a popular method for joining dissimilar materials (ferrous metals, non-ferrous metals, fiber-reinforced plastics, and others) [1]. It enables high performance and flexible joints while eliminating the weight and cost of fasteners (bolts, screws, rivets, etc.) associated with mechanical joining techniques. Nevertheless, the use of adhesives for multi-material joining has some challenges, which need to be addressed. The fact that automotive structural adhesives need to be heat cured poses a critical problem pertaining to the thermal expansion in substrates. The problem becomes more aggravated in case of multi-material joints pertaining to differences in the coefficient of thermal expansion (CTE) of the joined parts; the mismatch of which has significant implications on the integrity and response of the Body-in-White (BIW) to external loading.

To simplify the production process and for economic reasons, the adhesive heat curing process is combined with the paint baking process. At elevated temperatures in the paint baking oven, the different components of the body structure expand at different rates and magnitudes

depending on their different CTE and different air convection properties in local areas. After the adhesive is cured at the peak temperature, it constraints the thermal contraction in the components during the cooling down phase. This (when extended to all components and different joints in a BIW) leads to distortion in the structure, and more importantly residual stresses in the adhesive-bonded joints.

It is known that the presence of such residual stresses is detrimental to the performance of the adhesive bonds. It is experimentally established in previous publications by Reedy [2], Meschut [3], Ma [4], and Agha [5] that the process-induced residual stresses affect the performance of the adhesive-bonded joints. Several strategies and joint designs to mitigate the effects of residual stresses have been evaluated in the literature, such as the use of dual adhesives with complimentary high and low-temperature properties to reduce the stress concentration at the ends of the overlap by da Silva [6], or the use of functionally graded bondline by Carbas [7], and Marques [8].

Due to the absence of any direct and reliable experimental technique to measure the residual stresses in the adhesive bond [8], one of the main challenges here is the assessment of the nature and magnitude of residual stresses developing in the adhesive-bonded joint during the manufacturing process. Therefore, the use of adhesive-jointed

* Corresponding author.

E-mail address: aagha@clemson.edu (A. Agha).

multi-material structures in the body of an automobile is hindered by the lack of information on the value and extent of residual stress developed in the bond. It is, therefore, crucial to understand and consider the influences of heat-curing process induced stresses in the design of the adhesive joint and the body structure.

Several attempts have been made in the past to model the residual stresses in epoxy resins in carbon fiber composite structures to study the delamination behavior. Some works by Xiaogang [9], and Brauner [10] use an elastic constitutive model for that purpose, while some complex formulations by Ruiz [11], and Courtois [12] use viscoelastic models. Notable work has been done by Adolf and Martin [13] to calculate the stresses in crosslinking polymers depending on curing behavior. The basic idea in their work was to estimate the cure level and linking it to the mechanical properties of the polymer. It was also established later by da Silva [14] that automotive adhesives exhibit a small plastic behavior in addition to viscoelastic behavior which makes it difficult to directly adopt the existing models for automotive adhesives.

1.2. Framework of the study

This paper builds on the idea of using two distinct models for automotive adhesives, first for determining the degree of cure and second for predicting the mechanical behavior based on the calculated cure level. The goal of this work is to develop an efficient and easy to implement approach for characterization and modeling of adhesives during curing to predict the manufacturing induced effects on the adhesive joint. The proposed material model will enable the determination of the geometrical distortions in an automotive body structure generated due to the adhesive heat curing process and provides an estimation of the residual stresses developed in the adhesive bond. The prediction results for the manufacturing process-induced stresses from this model can be used as a starting point for component level and full-vehicle level crash simulations.

The application of the proposed adhesive curing model can also be extended to the innovative single-shot manufacturing process that has been recently developed by Kazan [15] to manufacture composite-metal hybrid components in one operation. The developed model in this work can be used to predict the final geometry of the hybrid part by calculating the distortion induced by this manufacturing process. Moreover, the calibrated material model can be fed into the numerical simulation of this hybrid process to determine the residual stress within the interfacial layer thus predicting the chance of delamination [16].

The next section introduces the theory and detailed formulation of the proposed material models – Curing Kinetics and Viscoelastic mechanical model. Section 3 presents the experiments – DSC, DMA and rheometer tests performed for calibrating the adhesive material models and the detailed mathematical approach to calibrate the material models. Section 4 discusses the finite element implementation and validation of the material model using a set of experiments involving curing of a single lap shear joint of a dissimilar and a similar substrate material combination. The last section also presents some unique outcomes of the simulation model, the modeling results agree with the experimental observations regarding the effect of bondline thickness and provide insights about the behavior of residual stresses in the joint.

2. Material modeling

When a BIW passes through a paint baking oven, different components of the structure are heated at different rates and extents depending on their thermal material properties, local air convection characteristics, design intricacy, and location of the component giving rise to non-uniform temperature-time histories across the component, which directly affects the uniformity of adhesive curing as shown by Dickie [17]. Since the mechanical properties of an adhesive bond are highly dependent on the quality of curing, it is crucial to accurately determine the degree of cure to accurately model the mechanical behavior of the

adhesive during curing and post-curing. Then, we need a mechanical model which can predict the mechanical properties of the adhesive depending on the degree of cure and temperature.

Adhesives are known to show viscoelastic behavior while they are being cured, and viscoelastic-plastic behavior after getting fully cured. In this study, it is assumed that the displacements due to CTE mismatch effects are small, due to which the adhesive sees only viscoelastic deformation. Therefore, the scope of this study is limited to the viscoelastic regime for simplicity. The model is purely viscoelastic and does not account the damages occurring in the paint oven due to CTE mismatch. It is well established that heat-cured adhesives exhibit chemical shrinkage on curing. It is also shown in several studies that the stresses generated due to chemical shrinkage are relatively small and their relevance for automotive applications is insignificant as compared to other phenomena, like CTE mismatch of substrates [8]. The measurement of shrinkage properties entails several tests on the Thermo-mechanical analyzer (TMA), which has been skipped from the scope of this study to reduce model complexity.

Hence, this work is divided into two models, (i) Curing Kinetics model and (ii) Viscoelastic mechanical model.

2.1. Curing kinetics model

The process of conversion of an adhesive from the viscoelastic liquid state to a viscoelastic-plastic state in the presence of a catalyst is called as curing of adhesive. As discussed earlier, the automotive grade structural adhesives are heat-cured adhesives, which need to be exposed to elevated temperatures for curing. When a thermosetting epoxy is heated, it undergoes a chemical reaction and gets cured to form a three-dimensional cross-linked network that is irreversibly locked in place and cannot be reformed or reprocessed. The degree of cure/conversion (represented as α) of an adhesive is a function of the temperature-time history that the adhesive is exposed to and is represented as a number ranging from 0 to 1. The rate of conversion with respect to time can be mathematically described as:

$$\frac{d\alpha}{dt} = f(\alpha) \cdot K(T) \quad (1)$$

where, $f(\alpha)$ is a phenomenological reaction model, while $K(T)$ is the temperature-dependent function defined by an Arrhenius relationship, which is:

$$K(T) = A \exp(-E_a/RT) \quad (2)$$

where A is the pre-exponential constant, E_a is the activation energy, R is the universal gas constant, and T is the temperature. The reaction model chosen for this work was Kamal's Model [18] which has been validated in several past studies by Zarrelli [19], Cai [20], Li [21], and Hu [22] based on epoxy resins.

Kamal's model is mathematically expressed in the following form:

$$f(\alpha) = (k_1 + k_2 \alpha^m)(1 - \alpha)^n \quad (3)$$

where, k_1 is the zero-conversion rate value, k_2 is the auto-catalytic rate constant, m is the auto-catalytic exponent, and n is the order of the reaction model.

2.2. Viscoelastic model

Adhesives are known to show time and temperature dependent viscoelastic behavior. The viscoelastic properties of an adhesive depend on the degree of cure, so the modeling approach was divided into two sections: (1) Viscoelastic model for fully cured material, (2) Degree of cure dependent viscoelastic model.

2.2.1. Viscoelastic model for fully cured material

The time and temperature dependent modulus of a thermorheolog-

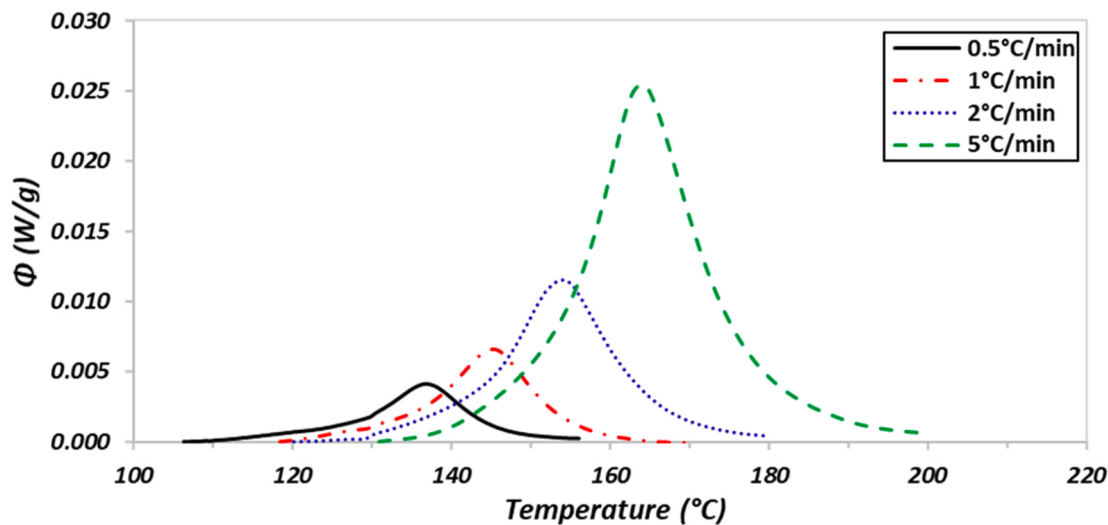


Fig. 1. Sample DSC heat flow scans normalized with specimen weight for different heating rates.

ically simple linear viscoelastic material at any temperature (within the range) can be estimated from the measured modulus at a known reference temperature by using the time-temperature superposition principle. The modulus vs. frequency curve at the reference temperature is known as the master curve, and the properties at a lower or higher temperature can be obtained by shifting the master curve left or right on the frequency axis, respectively. The discrete shift factors for each temperature are recorded and fit to a continuous mathematical model, required for modeling. Owing to its versatility to a wide range of polymers, the shift factors were fitted to Williams-Landel-Ferry (WLF) shift function [23] which is given by:

$$\text{Log}(\varphi(T)) = -A \frac{T - T_{\text{REF}}}{B + T - T_{\text{REF}}} \quad (4)$$

where, T_{REF} is the reference temperature at which the master curve was drawn, and the properties are known, T is the current temperature, while A and B are curve fitting parameters.

The master curve which is a representation of the relaxation behavior of the viscoelastic material can be modeled by Generalized Maxwell Model as previously done by Kaliske [24], Meuwissen [25] and Hossain [26]. The Generalized Maxwell model is mathematically expressed by Prony series expansion:

$$G(t, \alpha) = G_0(\alpha) \left(1 - \sum_i \frac{G_{i,\alpha=1}}{G_{0,\alpha=1}} (1 - e^{-\beta_i t}) \right) \quad (5)$$

where, $G_0(\alpha)$ is the instantaneous shear modulus as a function of the degree of cure, i represents the number of terms in Prony series expansion, $G_{i,\alpha=1}$ is the shear relaxation modulus for the i^{th} term for the fully cured material and β_i is the shear decay constant for the i^{th} term for the fully cured material.

2.2.2. Cure dependent viscoelastic model

The fundamental need in establishing cure dependence is to predict the instantaneous modulus at a certain cure level and an approximation of the relaxation behavior at that cure level. For this purpose, several authors have discussed the phenomenon of gelification. A resin's gel point represents a certain degree of cure which is associated with the start of the buildup of its mechanical properties [12] and it marks the stage when the polymer chains get enough crosslinked to act as solid and the resin no longer flows. Several authors assumed that below the gelation point, the adhesive is so compliant that the modulus is negligible and all the stresses are immediately relaxed [13,27]. However, after gelation, the stresses are not easily relaxed, and it marks the start of

residual stress buildup [28].

The approach used in this work is based on the work of Bogetti and Gillespie [29], who used a mathematical equation to determine the cure dependent equilibrium modulus using the degree of cure and full cure equilibrium modulus. The dependency of the equilibrium modulus will be approximated by using the following equation:

$$\mu_\infty(\alpha) = \mu_\infty(1) \left(\frac{\alpha^2 - \alpha_{\text{gel}}^2}{1 - \alpha_{\text{gel}}^2} \right)^{8/3} \quad (6)$$

where, μ_∞ is the equilibrium modulus at full cure, α_{gel} is the cure level at the point of gelification and α is the cure level at which the modulus is to be determined. For the sake of keeping the formulation simple and easy to calibrate, we will initially assume that the relaxation behavior at the time of curing is similar to the relaxation of fully cured material i.e., the temperature-dependent shift factors will be used for modeling. The gel point of the resin would be found mathematically by fitting the experimental properties to the model in equation Eq. (6). The consequences of this assumption will be evaluated in the experimental validation section of the paper.

The next section of the paper will discuss the experiments performed and the approach used in calibrating the discussed suite of material models.

3. Experiments for model calibration

The adhesive used in this work is an automotive grade structural adhesive Henkel Teroson EP 5089. It is a single component epoxy-based thermosetting adhesive.

Two sets of tests were run on the adhesive to calibrate the material models: Differential Scanning Calorimetry (DSC) to calibrate the curing kinetics model, and Dynamic Mechanical Analysis (DMA) to calibrate the viscoelastic mechanical model.

3.1. Calibration of the curing kinetics model

Adhesive curing is an exothermic process which means that energy is expelled when an adhesive is being cured. The energy released during curing of a thermosetting adhesive can be captured using DSC tests. This is achieved by exposing the uncured adhesive specimen to a controlled temperature ramp and analyzing the characteristics of the resulting exothermic cure peak while the adhesive cures in the DSC.

In this work, DSC measurements were performed using the DSC Q20 model from TA Instruments. Before the test, a specified weight of

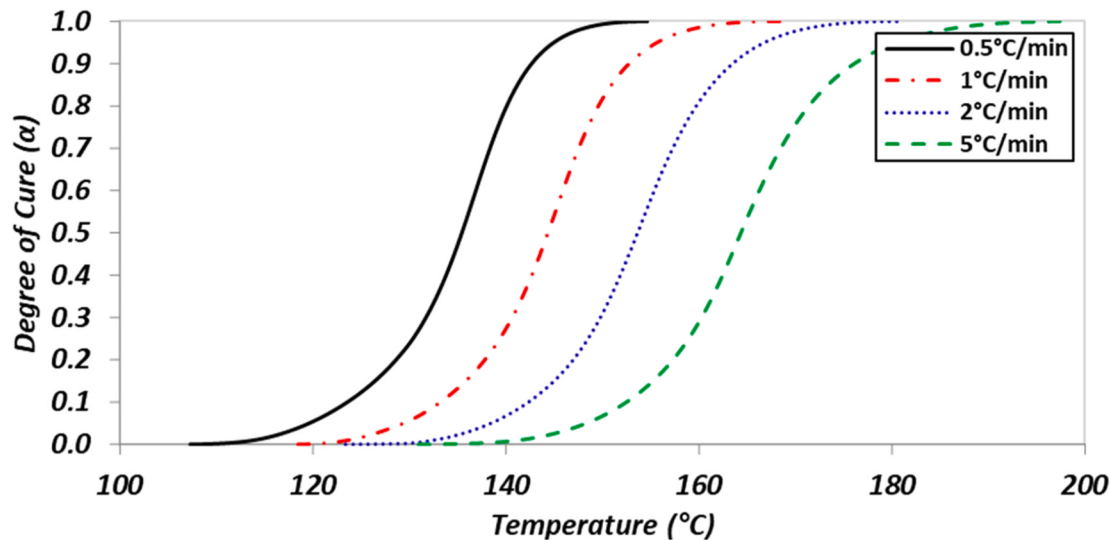


Fig. 2. Degree of cure vs. temperature obtained from DSC measurements on different heating rates.

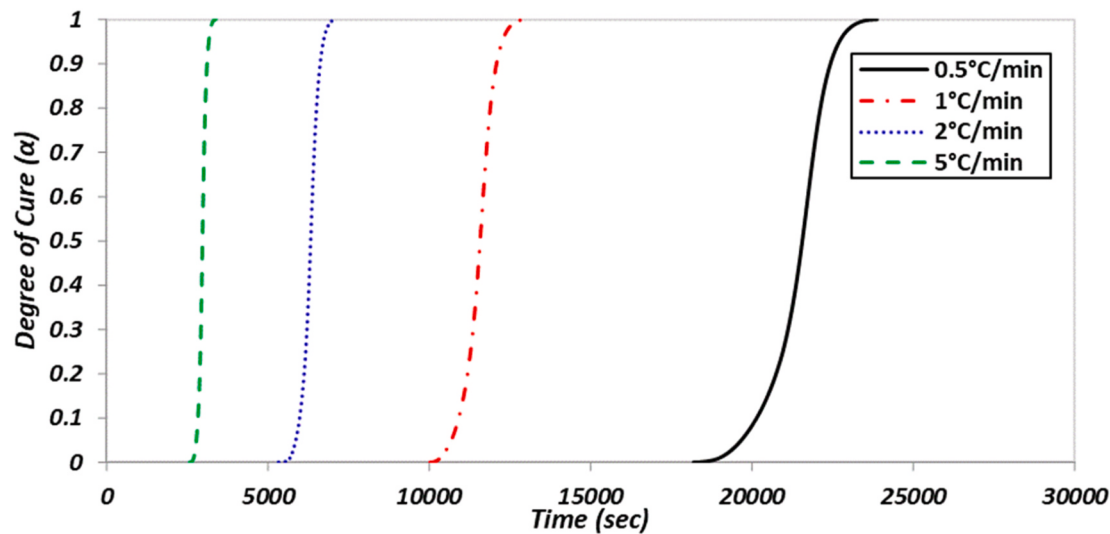


Fig. 3. Degree of cure vs. time obtained from DSC measurements on different heating rates.

Teroson EP 5089 EU adhesive was cooled in the machine from room temperature to -40°C for conditioning for at least 5 min. And then the DSC scans were run by heating the sample from -40°C to 250°C at constant heating rates of 0.5, 1, 2, 5, 10, and $20^{\circ}\text{C}/\text{min}$. DSC tests were also performed at isothermal conditions at 140°C and 160°C . A sample DSC map normalized with the adhesive weight for heating rates of 0.5, 1, 2, and 5 $^{\circ}\text{C}/\text{min}$ is shown in Fig. 1.

For the slowest heating rate, the onset of the cure peak for this adhesive is 110°C and the peak of the exotherm is located at approximately 130°C . As the heating rate increases, the onset of curing reaction and the peak of the bell curve move to a higher temperature. For Teroson EP 5089 EU, as per the data shown in Fig. 1, the total heat of the reaction i.e., the area under the curve divided by the heating rate is 185 J/g. The enthalpy results obtained from DSC tests did not vary too much for different heating rates and were found to be independent of the heating rate.

From the DSC measurements, it is now possible to determine the cure level assuming that the degree of conversion is proportional to the enthalpy generated by the reaction. If H_0 is the reaction enthalpy, ΔH is the heat generated in the curing process until a given time t , β is the heating rate and T is the temperature, then the degree of cure can be

defined by:

$$\alpha(t) = \frac{\Delta H}{H_0} = \frac{\int_0^t \varphi(t') dt}{\int_0^\infty \varphi(t') dt} \xrightarrow{dt=\beta dt} \frac{\int_0^T \varphi(T') dT'}{\int_0^\infty \varphi(T') dT'} = \alpha(T(t)) \quad (7)$$

Based on the above equation, the measured DSC results for EP 5089 were numerically transformed to give conversion level versus temperature and time as shown in Fig. 2 and Fig. 3, respectively. The same procedure was used to obtain the degree of cure for all the non-isothermal and isothermal DSC measurements.

It is a clear observation from Fig. 3 that the adhesive cures at a faster rate for a higher heating rate. This means that an adhesive can be cured faster by increasing the cure temperature. But, there is a physical limit to the maximum curing temperature, limited by the degradation temperature of the particular adhesive and increased adhesive shrinkage at higher temperatures [8].

The test data for heating rates of 0.5, 1, 2, and $5^{\circ}\text{C}/\text{min}$ was used for model calibration, while the results for heating rates of 10 and $20^{\circ}\text{C}/\text{min}$ and isothermal tests at 140°C and 160°C were used for the validation of curing kinetics model. The next task was to fit the experimentally obtained degree of cure curves to Kamal's model. In this

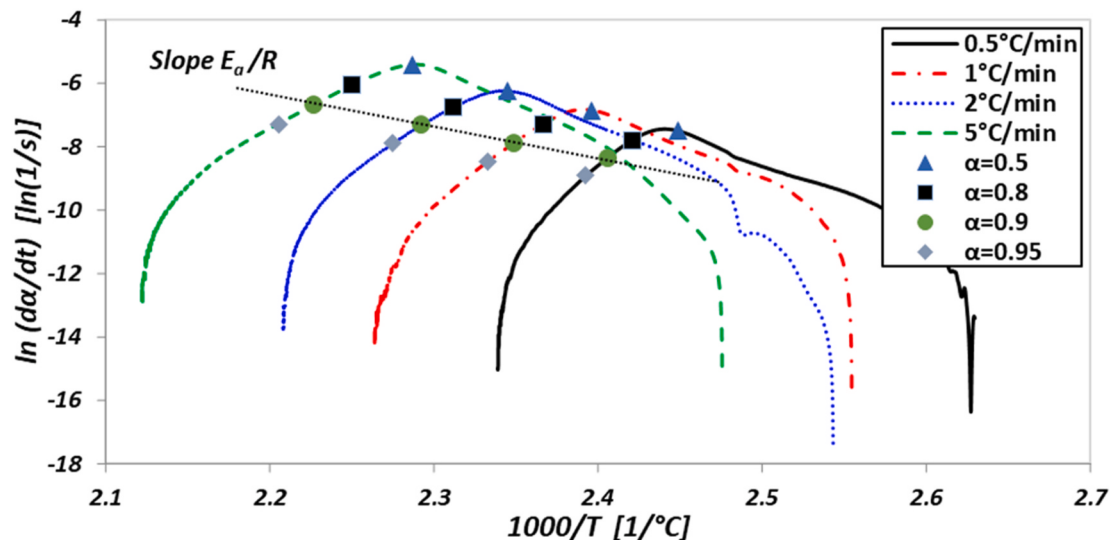
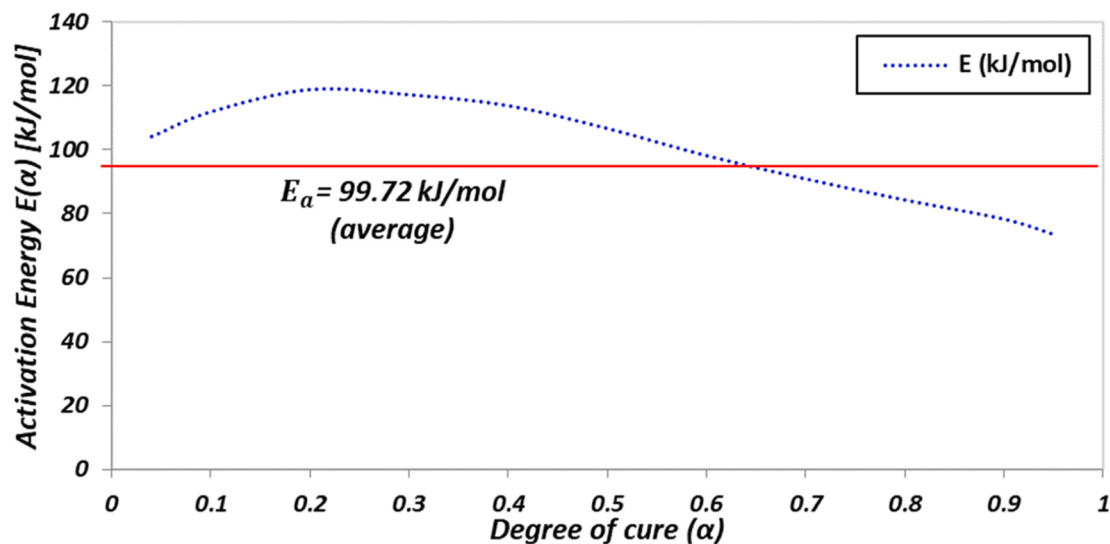
Fig. 4. Arrhenius plots and isoconversion line for $\alpha = 0.9$.

Fig. 5. Activation energy variation with cure level, average activation energy line.

approach, first, the activation energy of the reaction was calculated from the experimental data using the isoconversion method [20,21], using the logarithmic form of kinetics equation Eq. (1) combined with Eq. (2):

$$\ln \frac{da}{dt} = \ln[Af(\alpha)] - \frac{E_a}{RT} \quad (8)$$

The slope of $\ln \frac{da}{dt}$ versus $1/T$ for the same value of α gives the value of activation energy. The curves were drawn for cure levels ranging from 0.05 to 0.95. Then, isoconversion lines were drawn on the curves for different values of α and the slope was recorded. Fig. 4 shows the curves for different heating rates and isoconversion line drawn for a cure level of 0.9.

The activation energy of the reaction varies as the reaction progresses. The values of activation energy as a function of cure level are

shown in Fig. 5. The activation energy peaks in the middle and there is a visible drop in the energy at the beginning and at the end of the reaction. The trend of the activation energy can be attributed to the structure of the monomer, which results in cooperative motion of the chain segments in the beginning ($\alpha < 0.1$) followed by an increased activation energy for ($\alpha < 0.4$) owing to the increase in viscosity of the epoxy system which requires more energy to achieve the motion of the molecule chains. For $\alpha > 0.4$, the activation energy again decreases which was attributed to exothermic nature of the reaction resulting in sufficient mobility from the thermal energy during the curing process. The trend of the activation energy was similar to the trend observed by Cai [20] for a DGEBA-D230 system. For the sake of simplicity, average activation energy (99.72 kJ/mol) was used for further calibration. To determine the value of the remaining parameters, Eq. (1) was written in the following form:

$$\frac{da}{dt} e^{\frac{E_a}{RT}} = Af(\alpha) \quad (9)$$

With all the parameters on the left-hand side of Eq. (9) now known, a normalized plot for the left-hand side was drawn for each heating rate. The obtained curves were fit to Eq. (3) using non-linear regression and

Table 1
Calibrated parameters for curing kinetics model.

A	E_a	k_1	k_2	m	n
$e^{22.06}$	99.72 kJ/mol	0.26	5.16	1.15	1.46

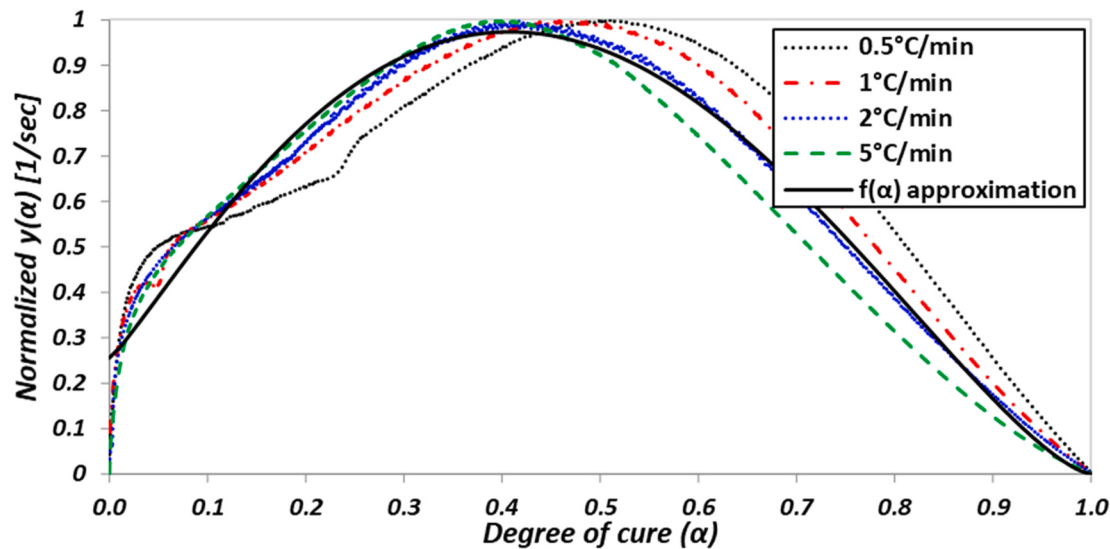
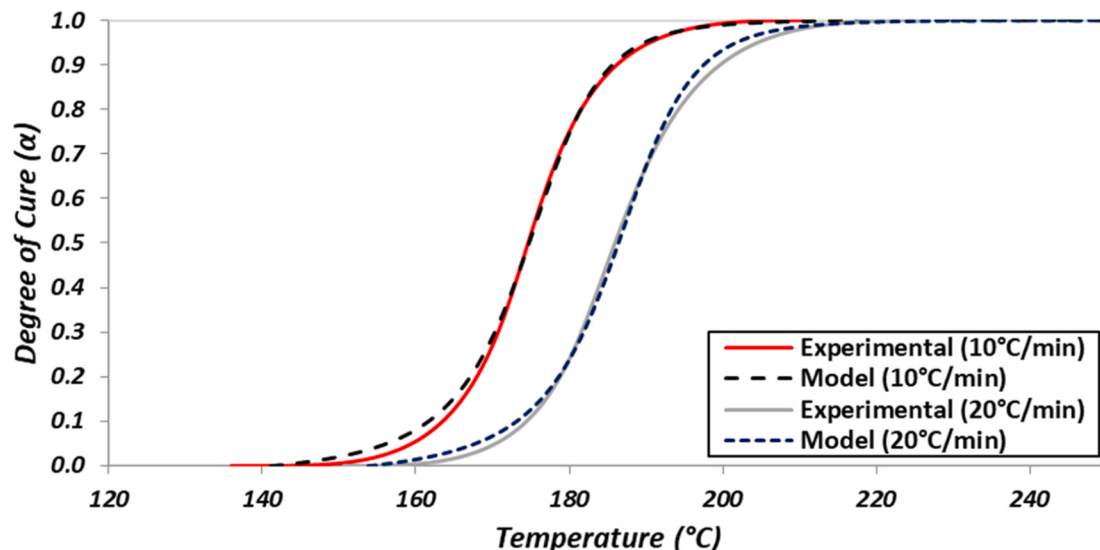
Fig. 6. Best fit $f(\alpha)$ curve fit curve for experimental curves.

Fig. 7. Comparison of model estimation vs experimental curves at the non-isothermal condition.

the best-fit curve parameters for $f(\alpha)$ were obtained. The values of the fitting parameters are given in Table 1 and the best fit curve is shown in Fig. 6.

The last parameter, pre-exponential factor A was found by scaling the $f(\alpha)$ approximation curve to the experimental data. The value of A is a function of the degree of cure. At the beginning and the end of the reaction the values of A which are calculated by Eq. (9) are not realistic because here the divisor $f(\alpha)$ is rather small and thus small deviations from the ideal curve shape have a strong impact on the value of A. Therefore, the average values in the conversion interval (0.01, 0.99) were taken. The optimized values of all the fitting parameters of the curing kinetics Eq. (1) are given in Table 1.

The curing kinetics model was calibrated for non-isothermal tests with heating rates of 0.5, 1, 2, and 5 °C/min. The calibrated model yielded good estimations for the experimental curing curves for heating rates of 10 and 20 °C/min and isothermal tests at 140 °C and 160 °C. The comparisons of the model estimation and experimental curves are shown in Fig. 7 and Fig. 8.

3.2. Calibration of viscoelastic model

3.2.1. Fully cured material

Henkel Teroson EP 5089, being an epoxy-based adhesive shows viscoelastic properties. The viscoelastic properties dependent on temperature and frequency were measured using a dynamic mechanical analysis system (DMA). The output of the DMA tests are viscoelastic moduli (storage and loss modulus) measured at different frequencies and temperatures. According to the theory of viscoelasticity, the real part of the modulus – storage modulus μ_S and the imaginary part of the modulus – loss modulus μ_L combine to form a complex modulus $\mu = \mu_S + i\mu_L$, where i is the imaginary unit number. The damping loss factor can be calculated by $\eta = \tan\delta = \frac{\mu_L}{\mu_S}$ where δ is the phase shift between the real and imaginary parts of modulus.

In this work, DMA measurements were performed with a bar in a torsional configuration. The DMA setup measures the stress vs. strain curve which can be used to calculate complex moduli. The modulus was obtained for a fully cured specimen for a combined frequency and temperature sweep, with a 0.1% strain amplitude, for a frequency range of 0.1 Hz–100 Hz, for a temperature range of −50 °C–200 °C at a step of

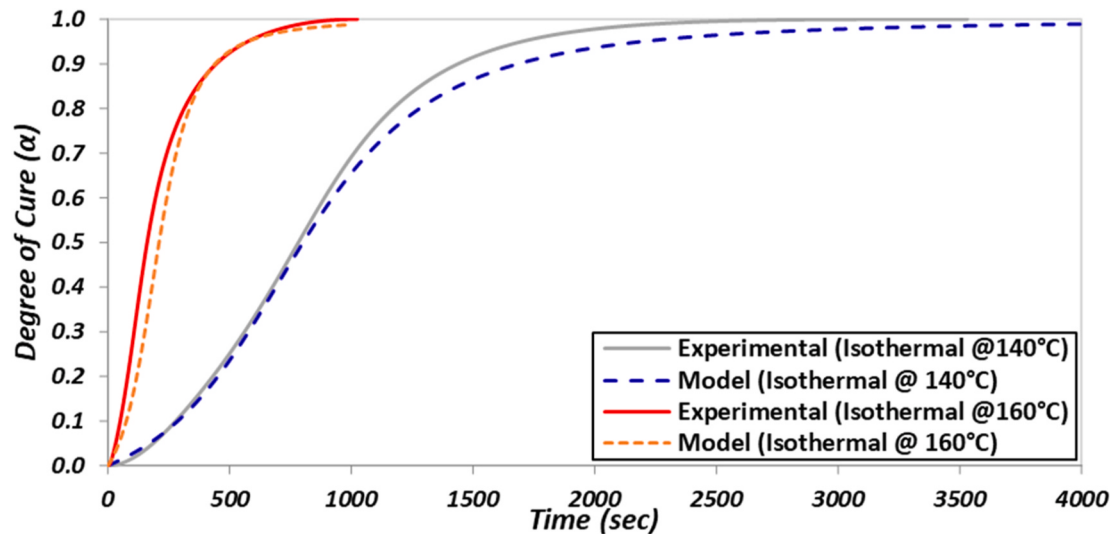


Fig. 8. Comparison of model estimation vs experimental curves at the isothermal condition.

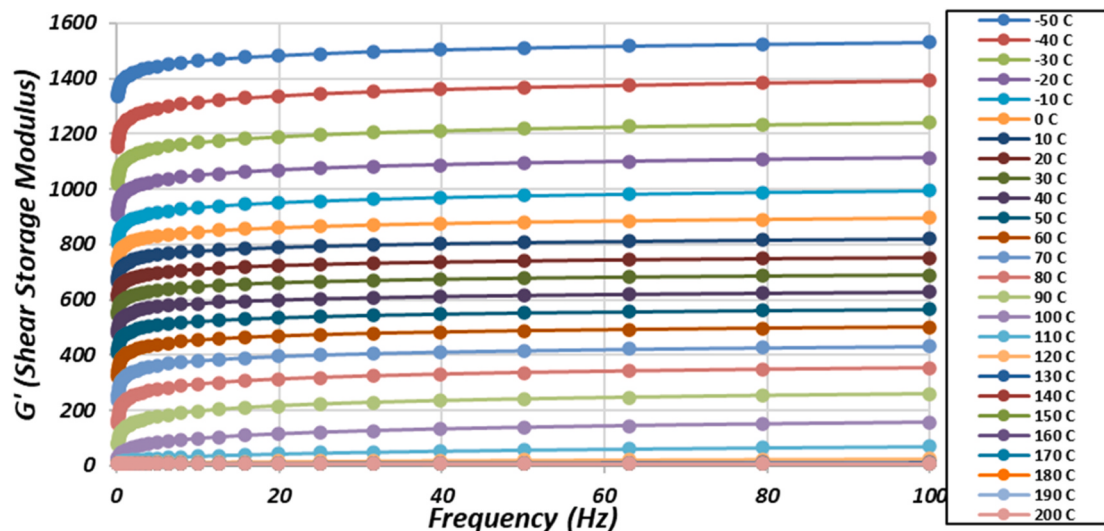


Fig. 9. Shear storage modulus vs. frequency as a result of combined temperature-frequency sweep.

10 °C. The storage modulus as a result of combined temperature and frequency sweep from DMA tests is shown in Fig. 9. As expected, it is visible that with a rise in temperature, the material softens, and the modulus decreases.

Using the time-temperature superposition principle applicable to linear viscoelastic materials, the modulus curves were shifted horizontally on the logarithmic frequency axis. For a reference temperature of 100 °C, the curves at higher temperatures in the lower portion of the plot were shifted to the left (to lower frequencies) and the curves at lower temperatures were shifted to the right (to higher frequencies), to generate a smooth continuous curve. The frequency shift factors obtained by manual shifting of the DMA curves were recorded for each temperature and were later fit to the WLF shift function, given in Eq. (4). The shifted modulus curve (known as the Master curve at 100 °C) drawn for storage, loss modulus, and loss factor is shown in Fig. 10. The scatter in the loss modulus values at higher temperatures is a result of phase changes in the material due to the actual temperature going beyond the glass transition temperature of the fully cured material. Here, the WLF shift function was overextended to fit over the glassy and the rubbery phase of the adhesive. This was done to simplify the model while making sure that the prediction results do not drift much from the

experimentally obtained storage and loss modulus at different temperatures.

The shift factors and the experimental master curve at 100 °C was fit to the models given in Eq. (4) and Eq. (5) respectively. The log of shift factors was fit to the WLF shift function using non-linear regression. A comparison of the experimental and estimated values is shown in Fig. 11. It suggests that the shift factor is negative for temperatures higher than 100 °C and positive for temperatures lower than 100 °C, which means higher temperatures shift to the right and lower temperatures shift to the left on the frequency axis. The calculated parameters for Eq. (4) are given in Table 2.

The developed master curve was fit to 16 terms of Prony series expansion using numerical techniques in scientific graphic and data analysis program OriginPro. It can be challenging to fit the storage modulus and loss modulus simultaneously to the Prony series. It was observed that transforming the master curve from frequency domain to time domain before fitting helps in the calibration of the model. The results of the best fit of the Prony series expansion to the experimental values are shown in Table 2 and Fig. 12. The storage modulus estimation by the model has a good overlap with the experimental values. The estimations for loss modulus and loss factor are wavy, which is typical for

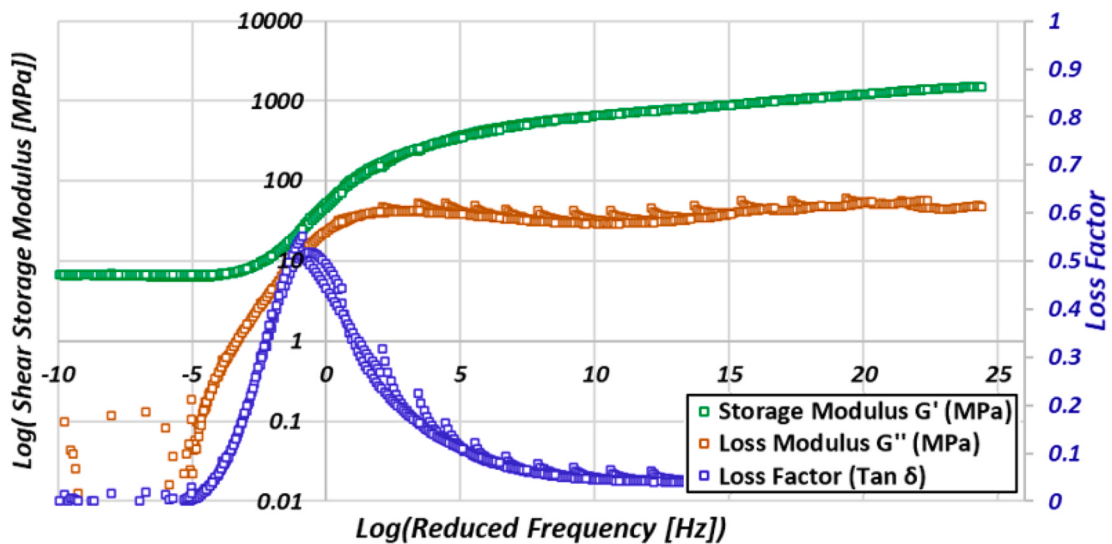


Fig. 10. Master curve showing shear storage, loss modulus and loss factor at 100 °C.

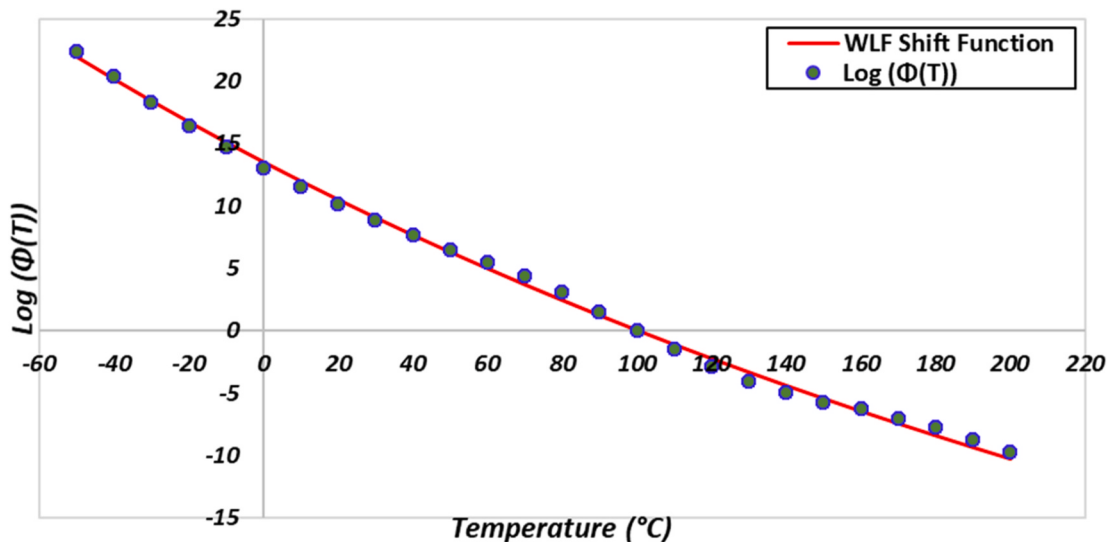


Fig. 11. Comparison of Log of experimental shift factors and WLF model estimation.

Table 2

Parameters obtained for best fit of WLF function: Eq. (4) and Prony series: Eq. (5).

	Shear Relaxation Modulus (G_i) [MPa]	Shear Decay Constant (β_i) [Hz]	Shear Relaxation Modulus (G_i) [MPa]	Shear Decay Constant (β_i) [Hz]
G1	119.0202	1.00E+24	G9	1.09E+02
G2	143.4906	1.00E+22	G10	1.34E+02
G3	153.1073	1.00E+20	G11	1.34E+02
G4	126.4329	1.00E+18	G12	1.30E+02
G5	131.2659	1.00E+16	G13	8.89E+01
G6	102.4958	1.00E+14	G14	1.56E+01
G7	91.12014	1.00E+12	G15	9.33E-01
G8	91.78917	1.00E+10	G16	1.00E-16
G_0	1577.67 MPa			
G_∞	6.63 MPa			
WLF	87.93			
A				
WLF	751.29			
B				

the Prony series expansion, but they represent the general trend of the experimental values satisfactorily.

According to the Prony fitting results shown in Table 2, the instantaneous modulus (G_0) of the material is 1577.67 MPa, while the long-term modulus (G_∞) of the material is 6.63 MPa. This means that the material relaxes with time and after a long time (~1E6 seconds) the modulus drops to 6.63 MPa.

The bulk modulus of the adhesive was calculated based on a Poisson's ratio of 0.4 (obtained from the technical specifications data sheet of the adhesive provided by Henkel) and the instantaneous shear modulus of 1577.67 MPa. For the sake of simplicity, the Poisson's ratio and the bulk modulus were taken to be independent of time and conversion, $K_\infty(\alpha) = K_0 = K_\infty = 7362.46$ MPa.

3.2.2. Cure dependent viscoelastic model

To capture the curing dependency of the material, rheometer tests were run on an uncured sample of the adhesive between two plates in torsional configuration at 0.3 rad/s oscillation with a 0.1% strain amplitude. The adhesive was cured in the rheometer while two sets of tests were run with dynamic temperature ramps of 5 °C/min and 10 °C/min from room temperature to 180 °C and 220 °C, respectively. The

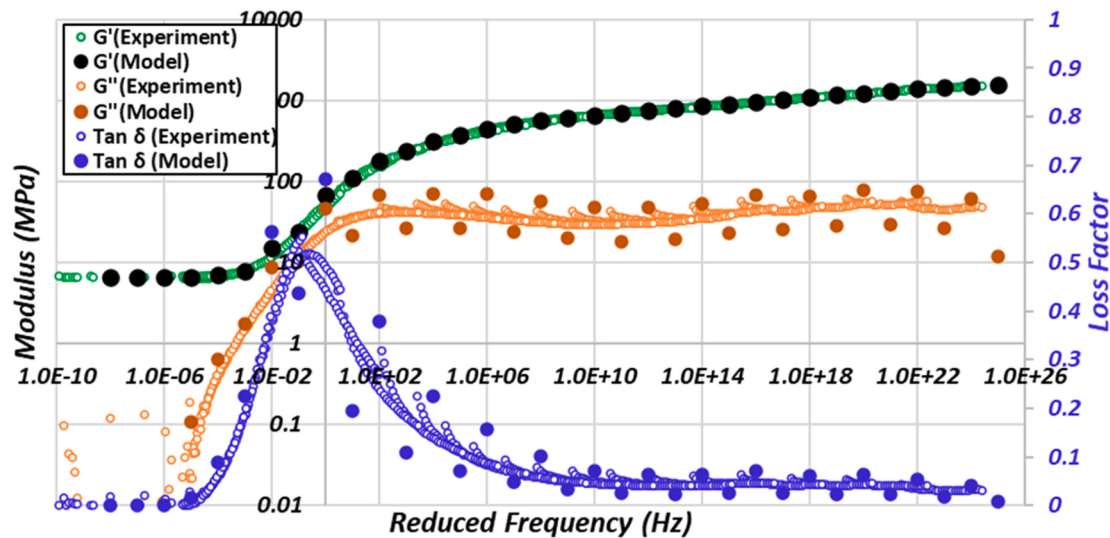


Fig. 12. Comparison of Prony series fitting vs experimental values.

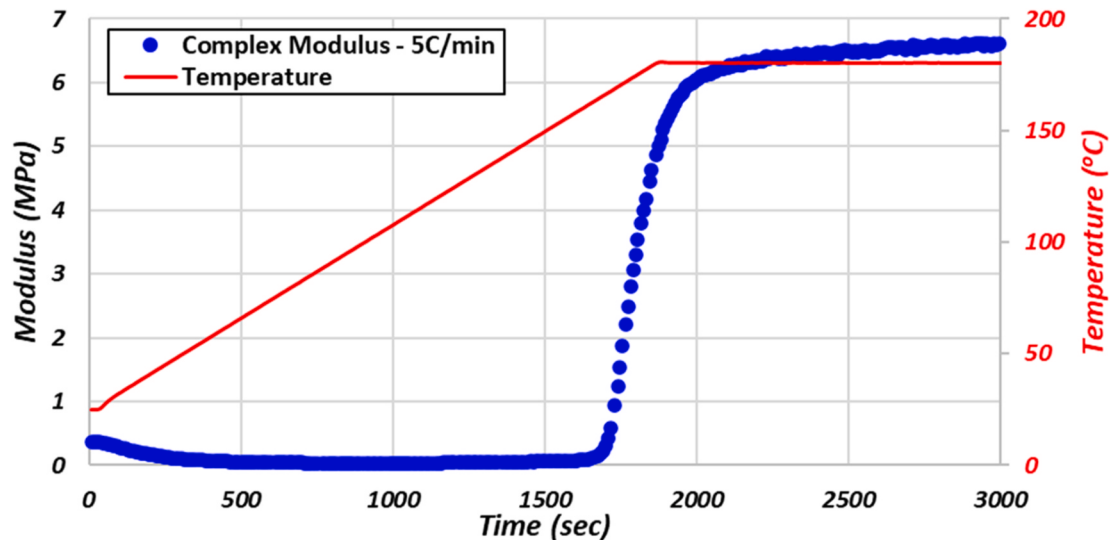


Fig. 13. Development of complex shear modulus with time for a temperature ramp of 5 °C/min.

measurement results are shown in Fig. 13 and Fig. 14.

The test data shows that the modulus for the uncured adhesive was negligible in the beginning and as the temperature increased with time, the adhesive gets cured and the modulus picks up and reaches a steady value which is close to the value of equilibrium modulus (6.63 MPa) previously calculated by Prony series for full cured adhesive, in section 3.2.1. The experimental results were transformed from modulus vs time and temperature to modulus vs cure using the curing kinetics model developed in section 3.1. The experimental results were fit to Eq. (6) and the best fitting for the data is obtained at $\alpha_{gel} = 0.56$ using the fully cured equilibrium modulus value of 6.63 MPa. Fig. 15 shows a comparison of the experimental results for modulus vs. cure along with the model estimation.

Thus, the adhesive material models consisting of (i) the curing kinetics model and (ii) the viscoelastic mechanical models were calibrated for EP5089. In the next section, the developed models will be validated for a unique experiment that was specially designed to capture the effects of CTE mismatch in the substrates during the adhesive curing process.

4. FEA implementation and experimental validation

4.1. Experiments for model validation

The experiments discussed by the author in a previous publication [5] were used to validate the material models developed for Henkel adhesive EP 5089. A special setup was built to allow the curing of an adhesive-bonded single lap shear joint specimen in the furnace, while the thermal displacements were being recorded using a 3D digital image correlation system and the force put on the joint was recorded.

There were three main outcomes of the experiments: (i) Y-Displacement across the joint, which is a measure of the increasing overlap area due to thermal expansion in the heating phase of the temperature cycle. (ii) Z-Displacement across the joint, which is a measure of the bending/distortion in the structure due to restriction in the contraction of the substrates in the cooling phase of the temperature cycle. (iii) Force applied by the adhesive bond to restrict the contraction in the substrates in the cooling phase, which is also responsible for the setting of residual stresses in the adhesive. The three output parameters for the two sets of experiments: (i) Dissimilar material joint of DP980-AA7071 and (ii) Similar material joint of AA7071-AA7071 were used

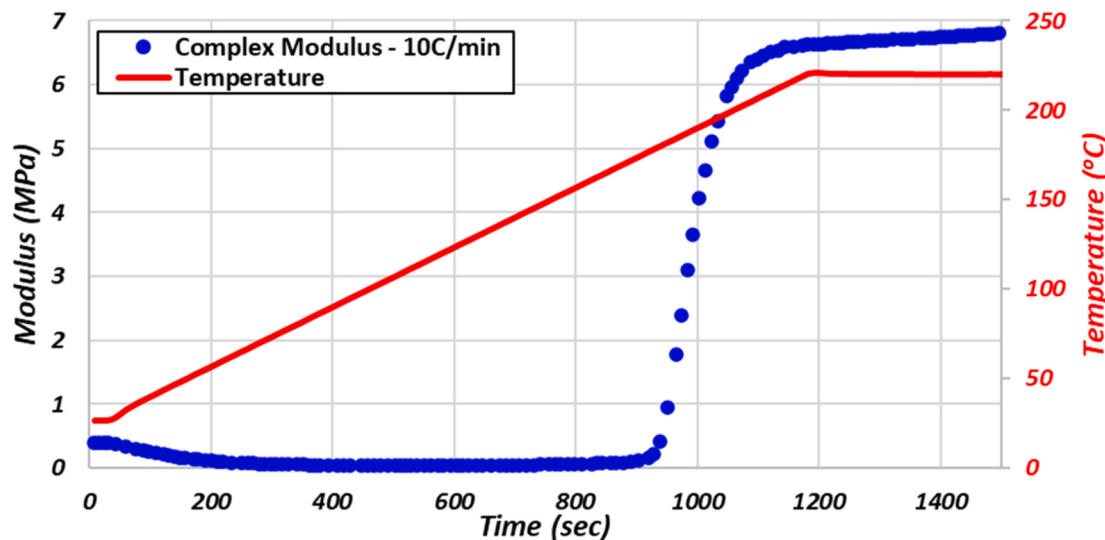


Fig. 14. Development of complex shear modulus with time for a temperature ramp of 10 °C/min.

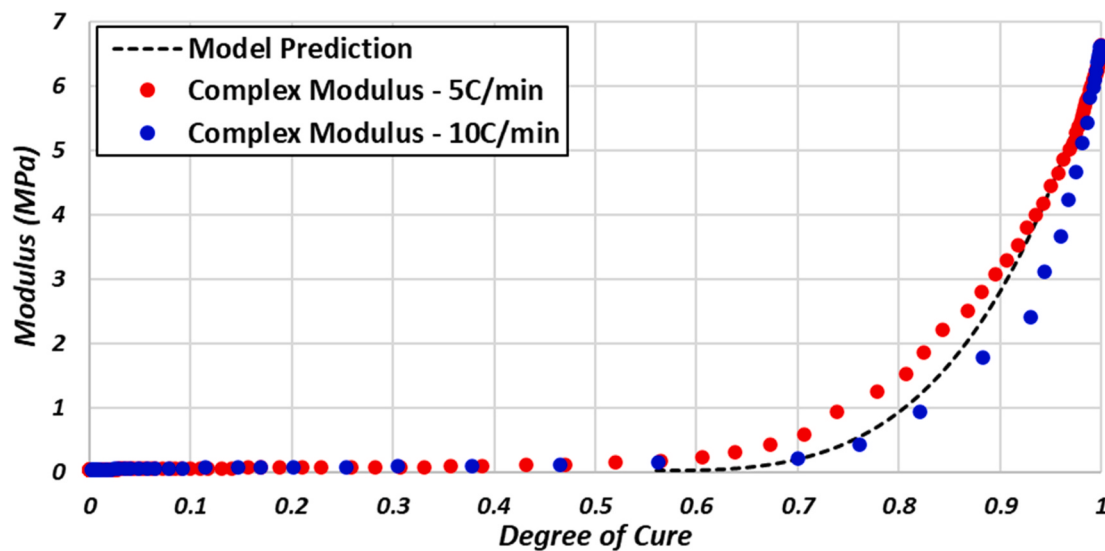


Fig. 15. Comparison of experimentally obtained modulus growth with cure vs model estimation.

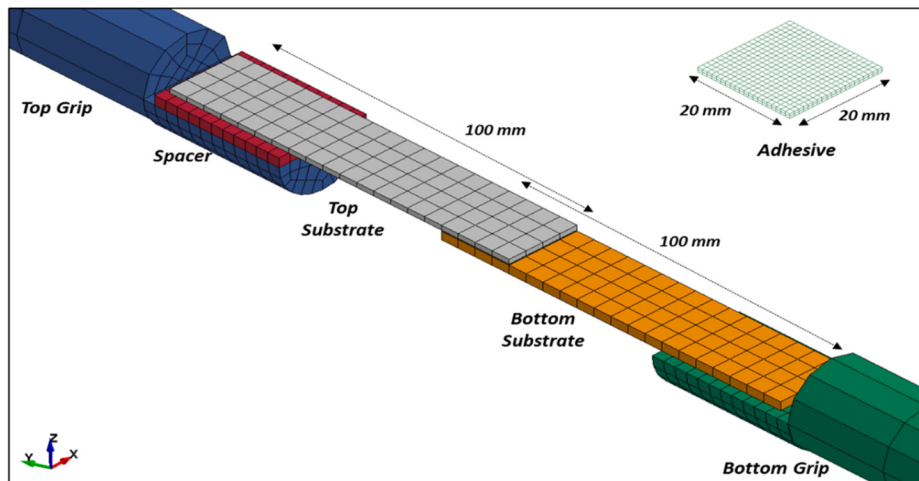


Fig. 16. Lap shear joint geometry used for the experiments and FE model.

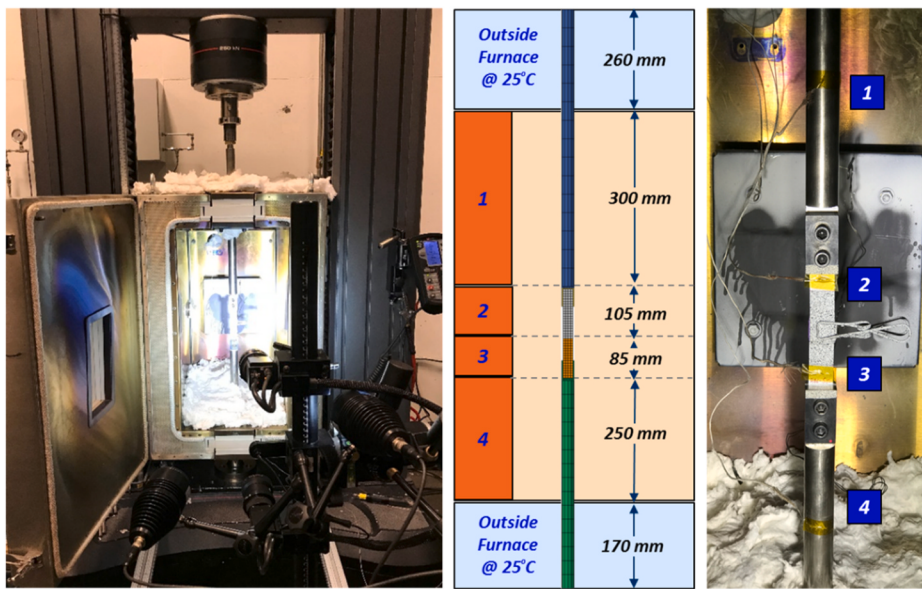


Fig. 17. Experimental setup; finite element model with 4 temperature regions carrying different temperature profiles; four thermocouples positioned on the grip rods and substrates.

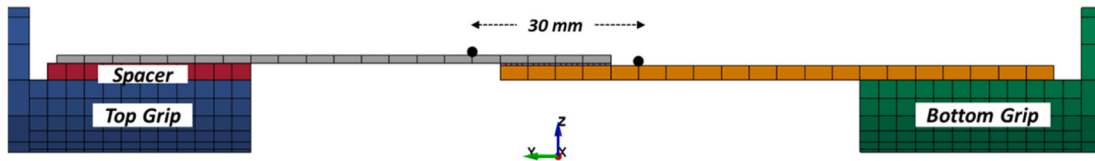


Fig. 18. FE model showing 30 mm extensometer across the joint.

to validate the adhesive material models.

4.2. Finite element model

4.2.1. Model geometry

Two simulation models were built in LS-DYNA to perform the experimental validation based on the experimental setup and two different substrate combinations: a multi-material combination of DP980 steel - AA7071 (ST-AL) and a similar material combination of AA7071-AA7071 (AL-AL). The simulation models consisted of six parts: Top and bottom grip rods made of Nickel-Iron (INVAR) alloy, top and bottom metal substrates (ST-AL or AL-AL), solid adhesive elements, and a top substrate spacer. The specimen dimensions were based on the experimental as shown in Fig. 16. The substrates were 100 mm long and 20 mm wide. The overlap length of the single lap shear joint was 20 mm. The thickness of the DP980 steel was 1.42 mm, and the thickness of the AA7071 substrate was 2.55 mm. Three simulations with varying adhesive bond thickness were done for each of the two substrate combinations to compare the effects of adhesive bondline thickness on the simulation results. A picture of the complete model geometry with the dimensions of the grip rods and temperature regions is shown in Fig. 17 and Fig. 18.

4.2.2. Boundary conditions

The grip rods were constrained at the top and bottom by fixing all six degrees of freedom. The curing cycle of the specimen was based on the data provided from the technical data sheet of the adhesive EP 5089. The actual temperature inside the baking oven was maintained at 180 °C for 40 min. Due to the design of the baking oven, the different regions of the furnace heat at different rates. To account for the variation in the

Table 3
Material properties for the substrates and INVAR grips used in the FE model.

Property	DP980 (@25°C - @200°C)	AA7071 (@25°C - @200°C)	INVAR (@25°C - @200°C)
Young's Modulus	204 GPa–196 GPa	64 GPa–52 GPa	137 GPa–126 GPa
Yield Strength	650 MPa–550 MPa	405 MPa–256 MPa	725 MPa–650 MPa
CTE	1.15E-5	2.18E-5	1.18E-6
Thermal Conductivity	55 W/m K	230 W/m K	20 W/m K
Density	7.87 g/cm ³	2.7 g/cm ³	8.2 g/cm ³
Poisson's Ratio	0.28	0.33	0.30

temperature profile, the experimentally obtained temperature profiles for the full baking cycle recorded for each test [5] from the four thermocouples were fed to the four regions of the simulation model as shown in Fig. 17. The parts of the top and bottom grip outside the furnace were given an initial temperature of 25 °C and were allowed to heat due to conduction from the inside. The actual duration of the temperature cycle was 200 min (40 min of heating followed by cooling phase) which was too long and computationally expensive with the typical time steps used for the solid adhesive mesh of size 1 mm. After a time scaling analysis, the simulation was time scaled by 1000x and the termination time was set to 12 s.

4.2.3. Model parameters

Solid elements were used for modeling the grip rods, substrates, and the adhesive bead. The metal substrates and grip rods were modeled using the material model *MAT_ELASTIC_PLASTIC_THERMAL which takes temperature-dependent properties of the material including

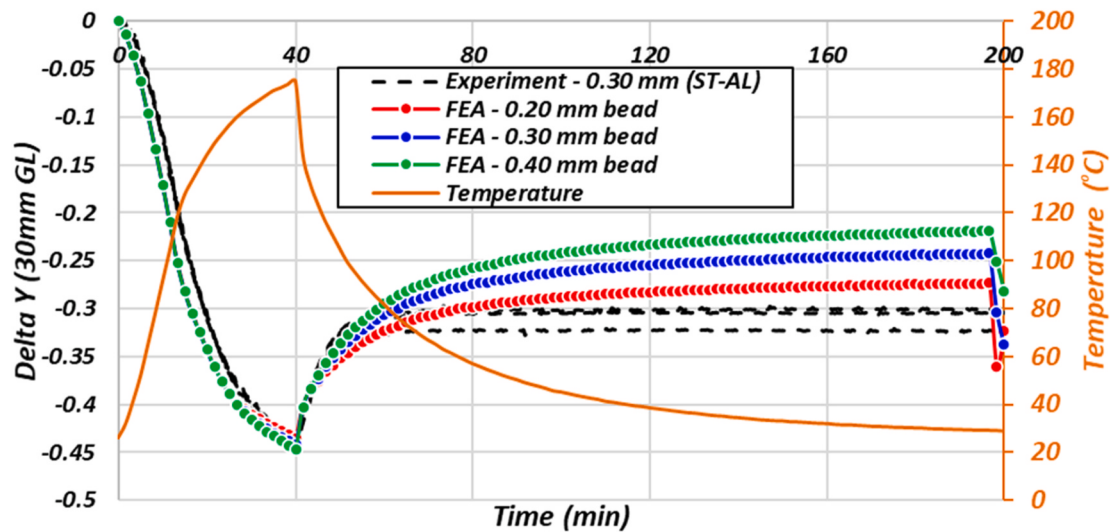


Fig. 19. Comparison of DIC measurements for relative displacement across the joint (ΔY) vs. FE estimation for ST-AL combination.

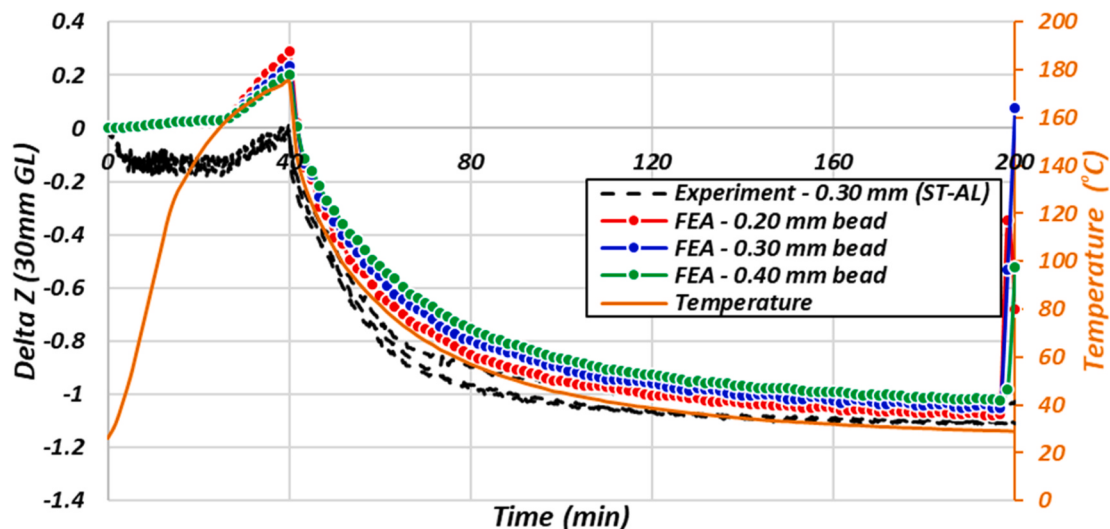


Fig. 20. Comparison of DIC measurements for bending distortion across the joint (ΔZ) vs. FE estimation for ST-AL combination.

coefficient of thermal expansion. The thermal material card used for the substrates, grips, and adhesive was *MAT_THERMAL_ISOTROPIC_TD_LC in LS-DYNA which takes the values for conductivity and specific heat capacity as a function of temperature. The material properties for the two substrate materials were obtained from tensile tests performed at room temperature and high temperature and are given in Table 3.

Adhesive Material Model in LS-DYNA: The adhesive material models developed in section 2 and 3 were adjusted to the pre-coded material card MAT_ADHESIVE_CURING_VISCOELASTIC (MAT_277) in LS-DYNA. The material card uses incremental strain to calculate Cauchy stress using a Stiffness matrix. The stress tensor for the next timestep is the sum of the purely elastic stress and a factor governing the viscoelastic contribution from each branch of the generalized Maxwell element. The frequency terms of the Prony series are shifted for the temperature effect using the shift factors given by the WLF shift function. The degree of cure given by the Curing Kinetics model is used to determine the equilibrium modulus, which is then used to scale the long-term shear relaxation modulus terms of the Prony series expansion. Agha [30] has given a detailed description of the formulation and FORTRAN implementation of the discussed curing kinetics and viscoelastic Maxwell model for a user-defined subroutine in LS-DYNA.

A layer of null shell elements *MAT_NULL was used between the solid adhesive elements and the substrates to avoid negative volume errors. The adhesive elements were tied to the substrates using *CONTACT_TIED_SURFACE_TO_SURFACE contact definition in LS-DYNA.

4.3. Comparison of FE and experimental results

For comparison, the relative displacements in Y and Z direction on a 30 mm gauge length across the joint (as shown in Fig. 18) were obtained from the FE model. A cross-section was defined on the top grip in the simulation model and the force through the cross-section was recorded for comparing with the experimentally obtained values. ΔY represents the relative displacement of substrates across the joint, while ΔZ represents bending distortion across the joint.

4.3.1. Multi-material bond of ST-AL

A comparison of the Y-displacement, Z-displacement, and force for ST-AL simulation models for varying thickness as compared to experimental data is shown in Figs. 18–20.

During the heating phase of the temperature cycle, the grips and the substrates expand and move relatively closer to each other therefore

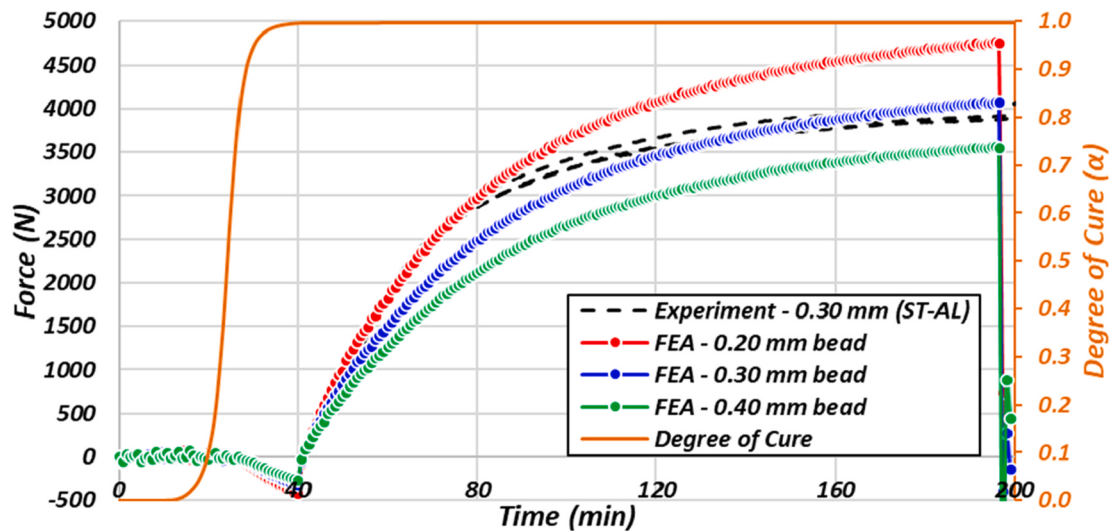


Fig. 21. Comparison of experimentally measured force vs. FE estimation for ST-AL combination.

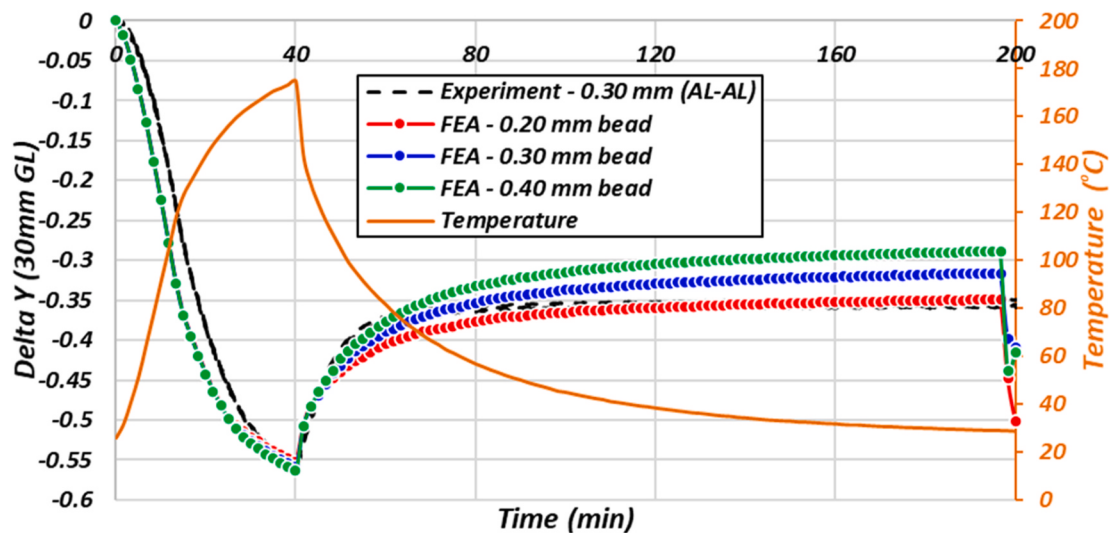


Fig. 22. Comparison of DIC measurements for relative displacement across the joint (Delta Y) vs. FE estimation for AL-AL combination.

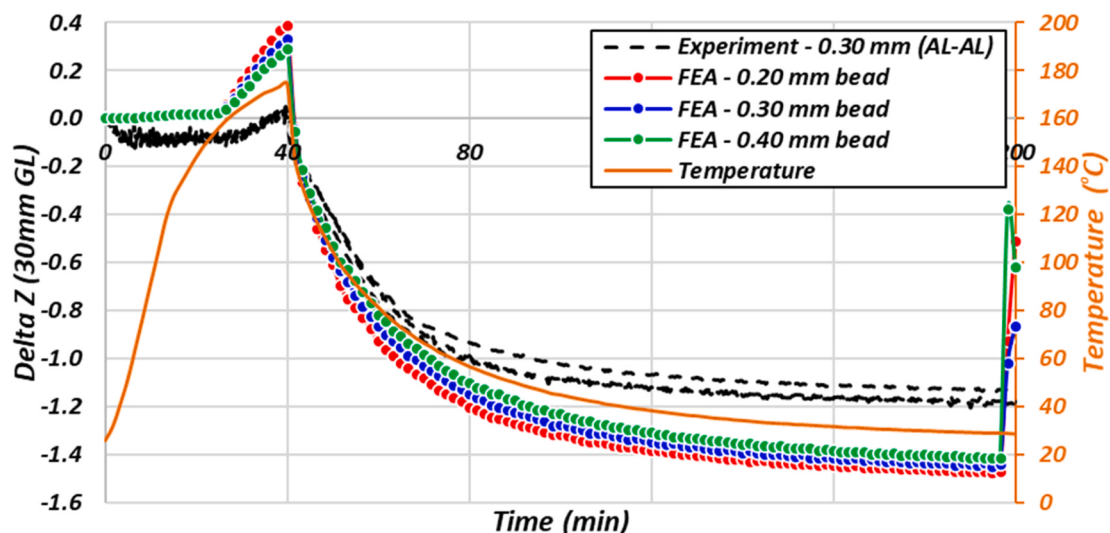


Fig. 23. Comparison of DIC measurements for bending distortion across the joint (Delta Z) vs. FE estimation for AL-AL combination.

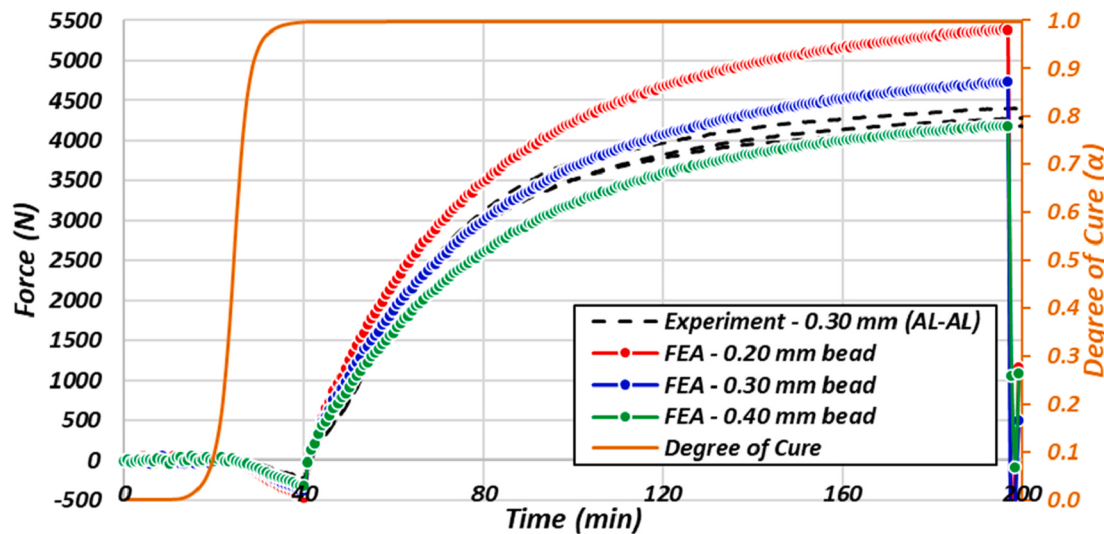


Fig. 24. Comparison of experimentally measured force vs. FE estimation for AL-AL.

giving a negative Delta-Y across the joint as seen in Fig. 19. During the temperature ramp, the adhesive is in an uncured liquid state and does not show any restriction to the thermal expansion of substrates which agrees with the initial zero force values in Fig. 21. At around 30 min, as the adhesive slowly cures and reaches the gelification point, the partially cured adhesive starts opposing any further expansion in the substrates and therefore picks up negative forces. At 40 min, when the cooling cycle starts, the substrates begin to contract and move away from each other, showing a positive relative displacement across the joint. At this point, now fully cured adhesive restricts the thermal contraction in the substrates and as a result, picks up positive forces as shown in Fig. 21. Therefore, the substrates do not return to their initial position generating distortion in the geometry and bending across the joint giving a residual Delta-Y and Delta-Z at the end of the cooling cycle as shown in Figs. 19 and 20. The force applied by the adhesive bond gives rise to residual stresses in the adhesive.

The model prediction for Y-displacement, Z-displacement, and force is in good agreement with the experimentally obtained data. As per Fig. 19, the FE results for 0.30 mm thick adhesive show a delta-Y of -0.25 mm against the DIC obtained value of -0.30 mm. Fig. 20 shows an estimated delta-Z value of -1.05 mm against the experimental value of -1.10 mm. Fig. 21 shows a close estimation of the final force value of

~ 4000 N at the end of the temperature cycle. It is to be noted that the experiments were performed at high temperature inside a furnace, where the heat waves cause a lot of distortion leading to some error in the DIC measurements. The small discrepancy between the experimental and predicted results may be due to the plastic effects in the adhesive which were ignored in the formulation. Considering the small magnitude of displacements, the overall range of displacements in the experiments and the FE simulation is in excellent agreement.

4.3.2. Similar material bond of AL-AL

A comparison of experimental vs. predicted results for the Y-displacement, Z-displacement, and force for AL-AL simulation models for varying thickness as compared to experimental data is shown in Figs. 22–24. The relative displacement in the aluminum-aluminum joint is larger than in the steel-aluminum joint owing to a higher CTE value for aluminum. The maximum delta-Y (at the peak temperature) is -0.56 mm for the AL-AL joint as compared to -0.45 mm for the ST-AL joint. A higher maximum relative displacement produces a higher residual delta-Y and delta-Z along with a higher force measurement. Another reason for higher delta-Z value is a lower young's modulus value of AA7071 as compared to DP980 steel.

The FE model prediction for Y-displacement, Z-displacement, and

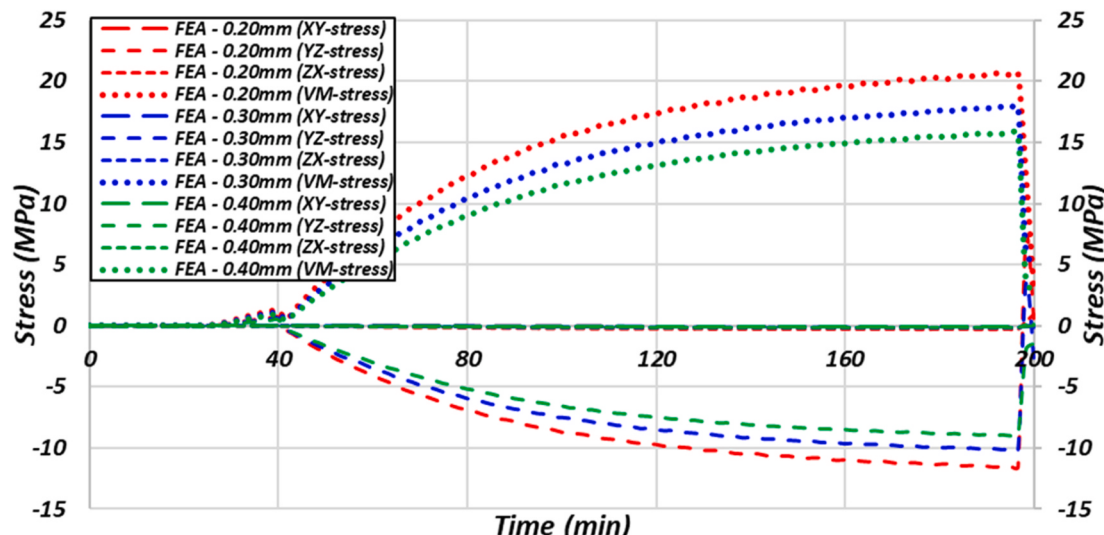


Fig. 25. FE model prediction of residual stresses for 0.2 mm, 0.3 mm and 0.4 mm adhesive bead for ST-AL.

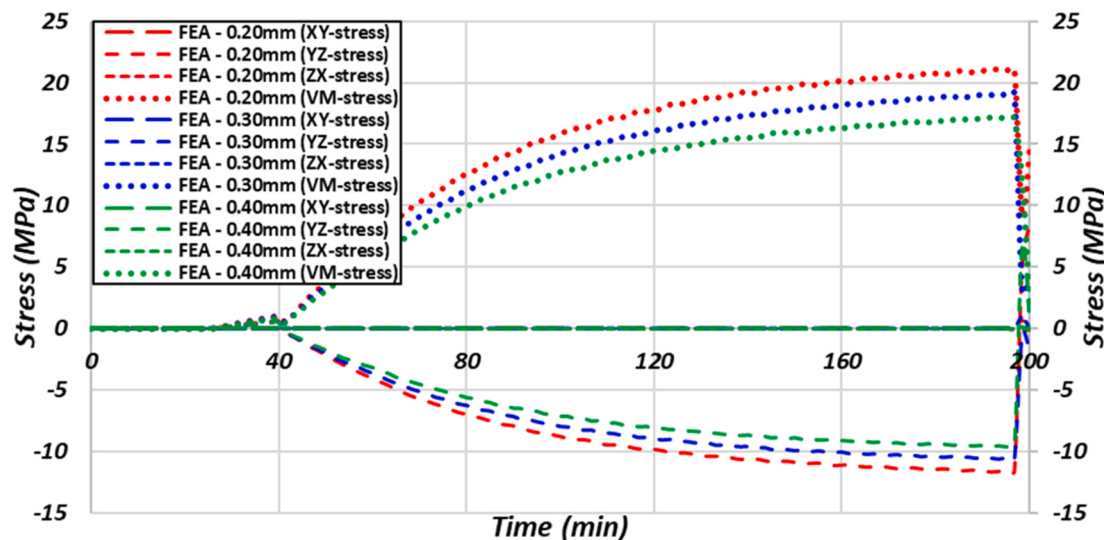


Fig. 26. FE model prediction of residual stresses for 0.2 mm, 0.3 mm and 0.4 mm adhesive bead for AL-AL.

force is in good agreement with the experimentally obtained data. As per Fig. 22, the experimental curves lie between the two FE generated curves for 0.30 mm thick adhesive and 0.40 mm thick adhesive and show a delta-Y of approximately -0.35 mm. The model predicts a higher level of bending i.e., delta-Z across the joint as shown in Fig. 23. Fig. 24 shows that an excellent prediction of force is obtained for AL-AL bond with the experimental scatter lying between the predicted values for 0.30 mm and 0.40 mm thick adhesive i.e., ~ 4500 N at the end of the cooling cycle. Similar to the ST-AL combination, the overall range of predicted displacements and forces is in good agreement with the experimental results.

4.4. Computational results

The FE prediction for residual stress in the adhesive in different directions at a central element is shown in Fig. 25 and Fig. 26 for the two substrate combinations. The stresses are nearly zero in the beginning until it passes the point of gelification after approximately 30 min. At the onset of gelification, small shear stress in the YZ plane develops due to the relative displacement of the two substrates. Up to 40 min, the stresses remain small because the stiffness of the adhesive is low at high temperatures even though it is already fully cured. Then the cooling phase starts and the displacement reverses its direction. The two substrates experience thermal contraction and start pulling each other through the adhesive layer, thereby inducing stresses in the adhesive. As a result, the shear stress changes its direction, and the effective stress shows the corresponding deflection point. As the temperature of the system decreases, the stiffness of the adhesive increases, and the residual stresses are set in the adhesive bond. The YZ-stress in the bond lies in the range of 10 MPa and the effective Von-Mises stress reaches approximately 18 MPa. The stresses in the XY and ZX direction remain close to zero due to very small displacements in those directions.

The stress levels in the AL-AL joint show slightly higher values owing to higher thermal displacements in the aluminum substrate.

Effect of thickness: The finite element results for the different adhesive bead thicknesses show interesting outcomes. With a decreasing adhesive thickness, the joint behaves stiffer, and as a result, produces greater residual displacement in delta-Y and delta-Z along with a higher force value. Subsequently, the adhesive bead thickness influences the residual stresses in the adhesive bond. A contour plot of the Von Mises effective stress in the substrates and the adhesive bond with different thicknesses is shown in Fig. 27. The modeling results show that increasing the bondline thickness is a way of reducing the residual stresses in the

adhesive and the overall joint. However, a thick adhesive bond negatively affects the overall rigidity of the structure. Therefore, an optimization of bondline thickness is desirable which can balance the global rigidity of the structure while minimizing the residual stresses in the joint.

5. Concluding REMARKS

This paper addresses the problems associated with CTE mismatch induced in adhesive-bonded multi-material structures. This work developed a suite of material models that work in conjunction to predict the effects of heat curing on an adhesive joint. The curing kinetics model predicts the degree of cure of the adhesive based on its temperature-time history. The degree of cure alpha is then fed into the viscoelastic mechanical model which defines the stiffness of the adhesive depending on the cure level, temperature, and relaxation in time. The models were calibrated for an automotive grade structural adhesive using DSC, DMA and rheometer test results. A unique set of experiments using 3D DIC were performed on a single lap shear joint of a dissimilar and similar material substrate combination. The calibrated material models were implemented into finite element models of the experimental setup for two sets of substrates.

The in-plane and out-of-plane displacement of the substrates across the joint, and the force exerted on the substrates were used to compare the FE model to the experiments. The overall range of predicted displacements and forces showed good agreement with the experimental results. The displacements and force in an AL-AL joint was higher than a ST-AL joint due to higher CTE. As a result, the residual stresses in an AL-AL joint were higher than a ST-AL joint. Another interesting outcome of the study was the effect of adhesive thickness on the residual stress level. It was validated that a thicker adhesive bond-line lowers the residual stresses in the substrates and the adhesive layer, however it compromises the overall rigidity of the structure. On the other hand, a thin bond leads to a stiffer joint and causes higher residual stresses in the adhesive-bonded joint. Considering the assumptions made in the modeling, the developed approach based on only the viscoelastic modeling of adhesives gives satisfactory results at the coupon level and can further be tested on a component or full vehicle level. It will also be interesting to model the plasticity and the aging behavior of the adhesive joint in a future study.

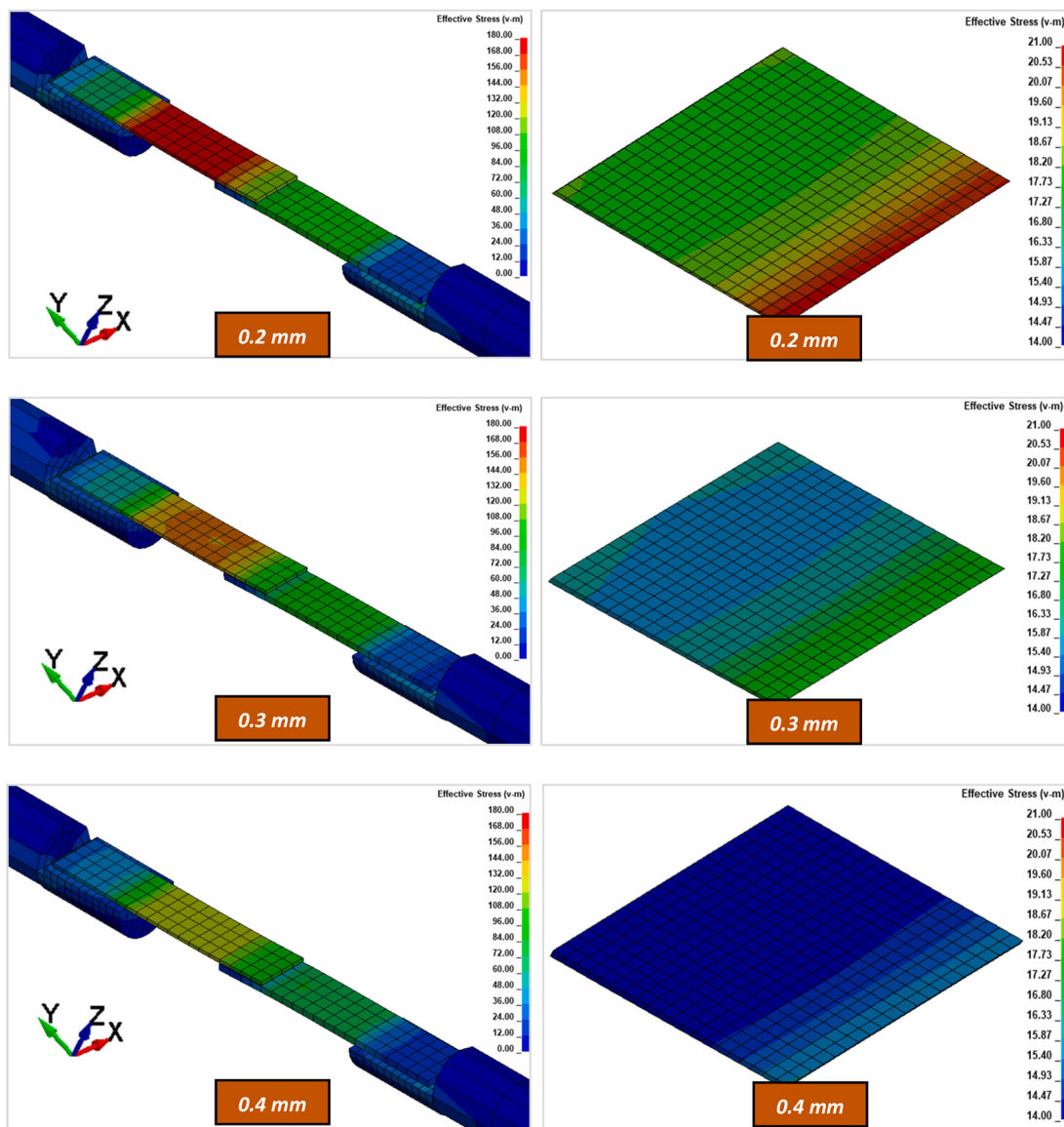


Fig. 27. FE predicted contour plots of effective stress in the substrates(left) and residual stress in the adhesive(right) for (i) 0.2 mm, (ii) 0.3 mm, and (iii) 0.4 mm adhesive bead (top to bottom) for ST-AL.

Declaration of competing interest

The authors declare that they have no known competing financial interests or personal relationships that could have appeared to influence the work reported in this paper.

Acknowledgements

We are thankful to the project sponsor Henkel Technologies, MI, USA for providing us with adhesives and supporting the study.

References

- [1] Banea MD, da Silva LFM. Adhesively bonded joints in composite materials: an overview. *Proc IME J Mater Des Appl* 2009;223(1):1–18.
- [2] Reedy ED, Guess TR. Butt joint strength: effect of residual stress and stress relaxation. *J Adhes Sci Technol* 1996;10(1):33–45.
- [3] Meschut G, Hahn O, Teutenberg D. Influence of the curing process on joint strength of a toughened heat-curing adhesive. *Weld World* 2015;59(2):209–16.
- [4] Ma C, et al. Study of the effect of curing residual stress on the bonding strength of the single lap joint using a high-temperature phosphate adhesive. *Materials* 2018; 11(7).
- [5] Agha A, Abu-Farha F. Experimental methods to capture curing induced effects in adhesive bonded joints. *Int J Adhesion Adhes* 2021;104:102735.
- [6] da Silva LFM, Adams RD. Adhesive joints at high and low temperatures using similar and dissimilar adherends and dual adhesives. *Int J Adhesion Adhes* 2007;27(3):216–26.
- [7] Carbas RJC, Silva LFMD, Critchlow GW. Effect of post-cure on adhesively bonded functionally graded joints by induction heating. *Proc IME J Mater Des Appl* 2014; 229(5):419–30.
- [8] Marques EAS, et al. Adhesive joints for low- and high-temperature use: an overview. *J Adhes* 2014;91(7):556–85.
- [9] Xiaogang Huang JWJG, Bogetti Travis. Process induced stress for woven fabric thick section composite structures. *Compos Struct* 2000;49:303–12.
- [10] Brauner C, Bauer S, Herrmann AS. Analysing process-induced deformation and stresses using a simulated manufacturing process for composite multispar flaps. *J Compos Mater* 2014;49(4):387–402.
- [11] Ruiz T. Thermomechanical properties during cure of glass polyester RTM composites. *J Compos Mater* 2004;39(10).
- [12] Courtois A, et al. Viscoelastic behavior of an epoxy resin during cure below the glass transition temperature: characterization and modeling. *J Compos Mater* 2019;53(2):155–71. <https://doi.org/10.1177/0021998318781226>.
- [13] Douglas Adolf JEM. Calculation of stresses in crosslinking polymers. *J Compos Mater* 1996;30(1):13–34.
- [14] da Silva LFM, et al. Analytical models of adhesively bonded joints—Part II: comparative study. *Int J Adhesion Adhes* 2009;29(3):331–41.

- [15] Kazan H, Farahani S, Pilla S. Influences of process parameters on penetration in a hybrid single shot manufacturing of carbon fiber/epoxy-polypropylene structure. In: SPE-ANTEC; 2019. Detroit. MI.
- [16] Farahani S, et al. Numerical simulation for the hybrid process of sheet metal forming and injection molding using smoothed particle hydrodynamics method 2019;1.
- [17] Dickie RA, Bauer DR, Ward SM, Wagner DA. Modeling paint and adhesive cure in automotive applications. *Prog Org Coating* 1997;31:209–16.
- [18] Kamal MR. Thermoet characterization for moldability analysis. *Polym Eng Sci* 1974;14(3):231–9.
- [19] Zarrelli M, Skordos AA, Partridge IK. Investigation of cure induced shrinkage in unreinforced epoxy resin. *Plast, Rubber Compos Process Appl* 2002;31:377–84.
- [20] Cai H, et al. Curing kinetics study of epoxy resin/flexible amine toughness systems by dynamic and isothermal DSC. *Thermochim Acta* 2008;473(1–2):101–5.
- [21] Li G, et al. Curing kinetics and mechanisms of polysulfone nanofibrous membranes toughened epoxy/amine systems using isothermal DSC and NIR. *Thermochim Acta* 2010;497(1–2):27–34.
- [22] Hu J, et al. Isothermal curing kinetics of a flame retardant epoxy resin containing DOPO investigated by DSC and rheology. *Thermochim Acta* 2016;632:56–63.
- [23] Malcolm L, Williams RFL, Ferry John D. The temperature dependence of relaxation mechanisms in amorphous polymers and other glass-forming liquids. *J Am Chem Soc* 1955;77(14):3701–7.
- [24] Kaliske M, Rothert H. Formulation and implementation of three-dimensional viscoelasticity at small and finite strains. *Comput Mech* 1997;19:228–39.
- [25] Meuwissen MH, et al. Prediction of mechanical stresses induced by flip-chip underfill encapsulants during cure. *Int J Adhesion Adhes* 2006;26(4):212–25.
- [26] Hossain M, Possart G, Steinmann P. A small-strain model to simulate the curing of thermosets. *Comput Mech* 2008;43(6):769–79.
- [27] Khoun L, Hubert P. Cure shrinkage characterization of an epoxy resin system by two in situ measurement methods. *Polym Compos* 2010;31(9):1603–10.
- [28] Abouhamzeh Sinke, Benedictus. Prediction models for distortions and residual stresses in thermoset polymer laminates: an overview. *Journal of Manufacturing and Materials Processing* 2019;3(4):87.
- [29] Bogetti G. Process-induced stress and deformation in thick section thermoset composite laminates. *J Compos Mater* 1991;26(5).
- [30] Agha A. Cure dependent viscoelastic-plastic modeling of adhesives to capture CTE effects in multi-material structures. Clemson University; 2019.